Analysis and classification of the process-induced surface topography nonuniformities during laser remelting

Beyfuss, Daniel; Bordatchev, Evgueni V.; Tutunea-Fatan, O. Remus

Publisher's version / Version de l'éditeur:
https://doi.org/10.1016/j.procir.2022.08.007
Procedia CIRP, 111, C, pp. 673-678, 2022-09-06

Available online at www.sciencedirect.com

ScienceDirect

Procedia CIRP 111 (2022) 673–678

www.elsevier.com/locate/procedia

12th CIRP Conference on Photonic Technologies [LANE 2022], 4-8 September 2022, Fürth, Germany

Analysis and classification of the process-induced surface topography nonuniformities during laser remelting

Daniel Beyfuss[a,b], Evgueni V. Bordatchev[b,a,*], and O. Remus Tutunea-Fatan[a,b,*]

[a]*Department of Mechanical and Materials Engineering Western University, London, Ontario, N6A 5B9, Canada*
[b] *Automotive and Surface Transportation Research Center, National Research Council of Canada*
800 Collip Circle, London, Ontario, N6G 4X8, Canada

* Corresponding author. Tel.: +1-226-688-5604; fax: +1-519-430-7064. *E-mail address:* evgueni.bordatchev@nrc-cnrc.gc.ca, rtutunea@eng.uwo.ca

Abstract

Surface polishing by laser remelting (SP-LRM) uses the energy of a focused laser beam to remelt the thin top layer of the workpiece material in order to improve its surface quality by 3D topography smoothing. Visual observations of the experimentally-obtained remelted laser tracks revealed that the uniformity of the LRM surface topography highly depends on the stability of the laser-material interactions and initial surface topography. Two metrics of LRM topography were proposed to assess the LRM process stability: uniformity of the laser track contour and uniformity of the middle longitudinal profile. Several sub-areas of the LRM tracks with typical topographic nonuniformities were visually selected and their nonuniformity metrics determined. Two common types of surface topography nonuniformities characterized by distinctive geometric patterns were identified: those induced by the LRM process (excessively remelted material) and those affected by the surrounding initial surface topography. The obtained results open new research avenues toward the in-process estimation of the surface topography formation and evolution via online monitoring of the LRM process stability.

Keywords: Surface polishing; laser remelting; process stability; nonuniformity of surface topography

1. Introduction

Surface polishing by laser remelting (SP-LRM) is a postprocessing finishing method that uses the thermal energy of a laser beam tracked across the surface to reduce its surface roughness and waviness [1,2,3]. This is possible due to formation and control of a moving melt pool that allows for the redistribution of material across the workpiece surface. The quality of the LRM-finished surface is highly dependent on several process parameters such as laser power, tracking speed, focal distance and so on. The balance of these parameters affects the stability of the SP process leading to the formation of LRM surface nonuniformities that disrupt an otherwise low roughness surface [4].

This preliminary investigation will explore the different types of these nonuniformities and their associated metrics. Several experiments were performed with a variety of the LRM process parameters. The polished surface topography was then visually explored to locate subareas with nonuniformities for further analysis. This led to identification of two main types of topography nonuniformities that are the product of the LRM process instability. These areas were visually and statistically analysed for identification of features and numerical metrics that could assist the classification of surface nonuniformities, primarily for further research on LRM process optimization and control.

1. Experimental setup and methodology

2.1. SP-LRM process experimental set-up

The system used during the SP-LRM process relies on a combination of laser beam delivery optics, 2-axis laser scanner, and 3-axis motion system with a CNC control system. A 100 W

10.1016/j.procir.2022.08.007

continuous wave laser (YLR-100-SYLR-100-SM-CS from IPG Photonics Inc., USA) was used to deliver a beam wavelength of 1070 nm. An optical assembly consisting of a collimator, scanner (exelliSCAN 14, SCANLAB GmbH, Germany), and *f*-theta lens was used to focus the laser beam within a 100 mm x 100 mm working envelope. In addition, a camera adapter was attached to both an optical camera for area alignment of the laser beam on the workpiece surface and a thermographic camera for gathering thermographic data during the LRM process.

The thermographic MWIR camera (TACHYON 16K, New Infrared Technologies, S.L., Spain) can capture images at 2000 fps with 128x128 pixels with wavelengths ranging between 1 µm and 5 µm. The 3-axis motion system relied on linear drives for the X and Y-axis while the Z-axis was controlled by a ball-screw drive. For thermal stability, these components were mounted to a granite table as shown on Fig. 1. All CNC-controlled components (laser, scanner, stages) were connected to the Aerotech CNC motion control unit.

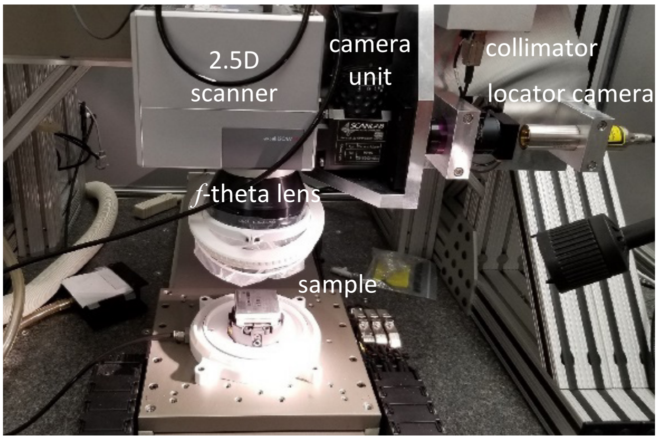

Fig. 1. Overall view of the SP-LRM experimental setup.

A 150 x 95 x 10 mm^3 sample made of ground H13 tooling steel was mounted on a System 3R rapid-clamping mechanism (Mikron AGIE Charmilles AG, Switzerland) attached to the Y-axis linear stage. This provided a repeatable and accurate (±1 µm) alignment that facilitated sample removal/ repositioning cycles for the purpose of surface topography measurements. A Renishaw touch probe was used to determine the focal position, set the working distance, and – if needed – measure the Z-deviation from the sample XY-plane. A custom-designed plastic shroud was placed around the *f*-theta lens and sample mounting fixture in order to maintain an Argon rich and oxygen-low environment.

2.2. Experimental procedure and analysis methodology

LRM process stability/instability analysis is based on the underlying assumption that a stable process yields a uniform topography. Following this hypothesis, any deviations from the uniform topography are induced by variations of the laser-material interactions. This is why it is desirable identify an input-output relationship between the LRM process and the surface topography of a complex thermodynamic system [5].

To address this, SP-LRM experiments and their analysis were performed in several steps. After laser tracks were produced by the LRM process, the topography of initial and remelted surfaces was digitized, nonuniform areas representing process instabilities were visually identified, the corresponding subareas were statistically analyzed, and their geometrical parameters were calculated. During the LRM experiments, eight 60 mm long laser tracks were generated perpendicular to the direction of surface ground marks. An overview of LRM track topography is depicted in Fig. 2 while process parameter combinations used are presented in Tab. 1. An optical profilometer (WYKO NT1100) having a 1 Å height measurement resolution and 0.258 µm/pixel resolution was used for the digitization of the 3D surface topography. This was accomplished by means of an autostitching procedure performed along the 60 mm length with which the final image is made of the mean value of three measurements.

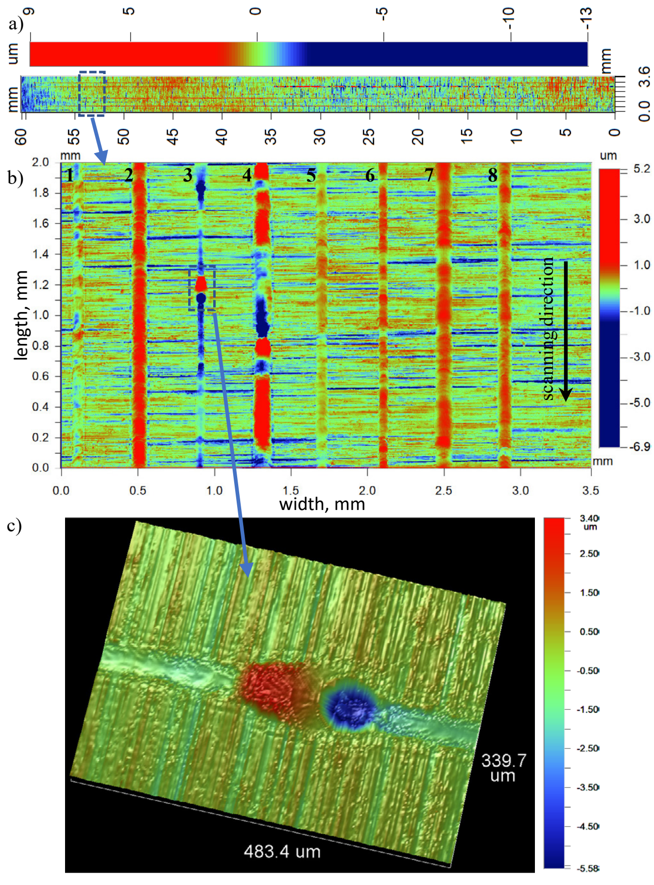

Fig. 2. 3D surface topography of experimentally-obtained laser tracks: a) overall area, b) typical detailed small sub-area, and c) typical instability under evaluation.

Table 1. LRM process parameters used during experiments

Line	1	2	3	4	5	6	7	8
Laser power (W)	15	20	20	25	30	30	40	40
Scanning speed (mm/s)	50	50	50	50	100	200	50	100
Focus offset (mm)	0.0	0.0	0.2	0.2	0.4	0.4	0.6	0.6

The next step of the methodology was the evaluation of the uniformity for the entire line. For this purpose, the surface topography of each line was obtained along its total length. Nonetheless, start and end acceleration/deceleration distances (~0.3 mm) were excluded [6]. Using this topographic data, several average characteristics can be calculated: average transversal profile, *h(width)*, roughness profile, $R_a(width)$, waviness profile, $W_a(width)$, root mean square profile, $R_q(width)$, standard deviation (STD) profile, $\sigma(width)$, and several others in accordance with ISO 4287 and ISO 4288 standards. These are general metrics of the LRM topography uniformity as well as LRM process stability along the laser track. In addition, the analysis of the SP-LRM process will include the assessment of statistical characteristics of the initial and LRM surface profiles, calculate their spectral densities, amplitude distributions, and their statistical interdependences as estimated by transfer and coherence functions [7].

At the same time, the STD value of the surface roughness for the centerline of the polished area and that of the initial surface were computed. The value of the centerline roughness for the initial surface is derived from the average value of the surface height on both sides of the polished line. This type of approximation is facilitated by the direction of the feed intentionally chosen to be perpendicular to the direction of the ground marks. In the current context, STD quantifies the number of values and their distance from the mean in each area and this makes it an accurate uniformity/nonuniformity metric.

In addition to the overall characteristics, the topography of each laser track was evaluated in detail in order to locate surface nonuniformities (such as sudden changes of the height and width) as well as irregularities of the LRM surface (Fig. 2c). However, the identification of the root cause for these rapid changes is not a trivial task. In an attempt to provide insight on this matter, high-speed thermographic imaging of the laser-material interaction zone was performed during polishing trials. This information is expected to enable a more comprehensive understanding of the correlation between process conditions and surface formation.

3. Analysis and classification of process stability

The process of surface polishing by laser remelting (SP-LRM) aims to generate a uniform and smooth surface topography by redistributing material in a molten state. This is attained by irradiating with a laser beam an initially rough and irregular surface. As it can be anticipated, LRM is not a thermodynamically and mechanically stable process primarily because of nonlinear, chaotic, uncontrollable micro- and macro- flows and fluctuations within the laser-material interaction volume. Therefore, it would be accurate to say that the LRM process itself is one of the principal sources of irregularity/nonuniformity in the remelted topography.

Under typical LRM conditions, five main types of process-induced surface structures can be identified: ripples, undercuts, bulges, step structures, and martensite needles [8]. The first three types in the list are those most affecting the final quality of the polished surface. In the past, formation of ripples was extensively investigated by researchers, mainly from the perspective of thermodynamic and hydrodynamic phenomena. Detailed experimental analyses of ripples (sometimes called surface periodical structures) [9-11] reveal that they are one of the important byproducts of the laser remelting. Ripples are formed during the surface over-melting regime when surface-tension gradients generated by the radially oriented melting-solidification temperature gradients start to pull in outward directions the top volume of the molten material. This leads to the formation of nonplanar meniscus waves. In addition to the already performed analysis of the ripples [9-11], this study focuses on the identification and preliminary analysis of the surface nonuniformities caused by the initial surface topology of the sample as well as those caused by unknown sources leading to sudden changes in the laser-material interaction.

In this context, it is proposed that the effect of the initial surface topography can be identified by analyzing its statistical correlation with the remelted topography. More specifically, initial surface topography directly affects the flow of the liquefied metal by directing it under the concurrent action of gravity and shear stresses. As expected, the flow happens from peaks to valleys that become filled with molten material.

On the other hand, rapid changes in laser-material interactions can be recognized as instantaneous modifications of the molten material volume and shape that cause the melt pool to suddenly become larger or smaller. Thermodynamic effects are caused by the relative imbalance between process parameters, particularly between conduction and convection temperature gradients. More specifically, if the laser beam moves too fast with respect to the given power and focal distance, the surface may not be able to absorb the applied energy in order to form a steady melt pool and therefore a uniform laser track. In this case – that might be regarded as an instance of under-melt – the material is being superficially melted by the laser energy applied during an extremely short laser-material interaction time. By contrast, in the case of low scanning speed and high laser energy, the molten pool is formed under the action of temperature gradients from the current laser-material interaction as well as from conduction-based temperature propagation from earlier polishing passes. This may yield a momentary loss and reformation of the melt pool that often leads to abrupt interruptions of the molten pool formation dynamics, excessive displacement of the resolidified material, formation of large bulges above the average surface height and/or local deep cavities. To confirm the existence of process instabilities described above, examples of topographic features will be identified and further analyzed.

3.1. Surface topography formation under stable remelting

The distinctive characteristics of surface topography under stable LRM are the constant width and consistent shape of the laser track along the longitudinal profile. These characteristics can also be identified in rippled surfaces. Fig. 3 illustrates a 3D surface topography and a subarea with typical ripple formation obtained under a stable LRM process. The topographic analysis was performed on line 2 in Tab. 1 (47 to 49 mm).

This is a resupply of March 2023 as the template used in the publication of the original article contained errors. The content of the article has remained unaffected.

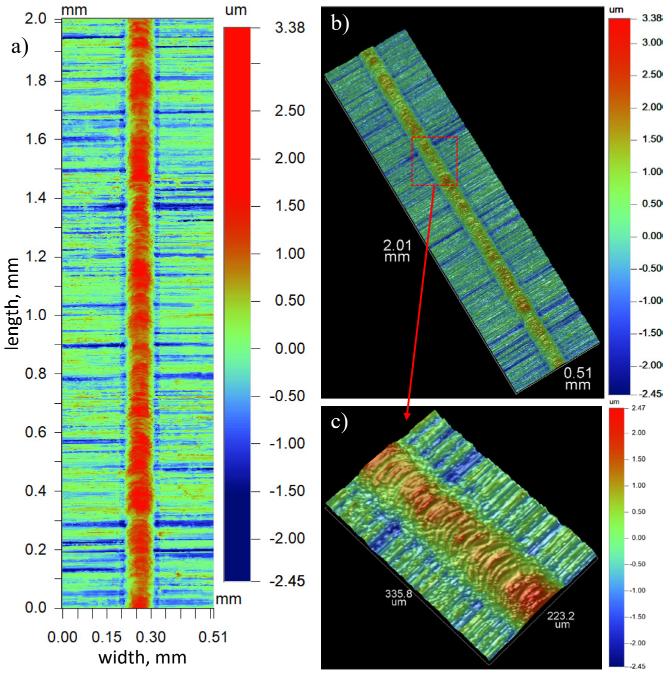

Fig. 3. 3D surface topography obtained under stable LRM process: a) top view, b) isometric view, and c) subarea with typical ripple formation.

Following this, several process metrics were obtained and analyzed according to the methodology described in Section 2.2. The stability of the LRM process was analyzed by calculating standard deviation values for longitudinal profiles of the initial topography and LRM topography at the center of the laser track (Fig. 4). The two values yielded as $\sigma_{ini} = 0.38$ µm and $\sigma_{LRM} = 0.27$ µm, respectively, and they correspond to the improvement of the surface quality from $R_{a,ini} = 0.31$ µm to $R_{a,LMR} = 0.22$ µm (29.0% improvement) and from $R_{q,ini} = 0.40$ µm to $R_{q,LMR} = 0.27$ µm (32.5% improvement). As Fig. 4 implies, no major irregularities are present in this case.

In addition to the metrics presented above, average transversal profiles, $h(y)$, $R_a(y)$, $R_q(y)$, $\sigma(y)$ were calculated along the laser track. Fig. 5 outlines $h(y)$ and $\sigma(y)$ profiles and Fig. 6 shows $R_a(y)$ and $R_q(y)$ profiles showing the distribution of the surface quality across the LRM laser track.

It is also necessary to emphasize that the $h(y)$ profile unveils two topography structures, namely undercuts and bulges having an undercut depth of -0.382 µm and a bulge height of 1.393 µm. This indicates the anticipated trend of an elevated post-polished profile that tends to pull material towards the centerline [12]. The pool also pushes the material backwards in a consistent material transfer. The bulge/elevated profile is associated with an overall increase in volume due to martensite formation [13]. The stable LRM process and its associated surface topography shows evident ripple formation due turbulent molten flow thermodynamics (Fig. 7).

3.2. Effect of initial surface features on topography formation

At certain remelting process conditions, sizable geometrical features (2-3 times larger than the standard deviation of the uniform initial topography) of the initial surface may affect the formation of the consistent laser tracks that are ideal for the achievement of the best/desirable surface quality.

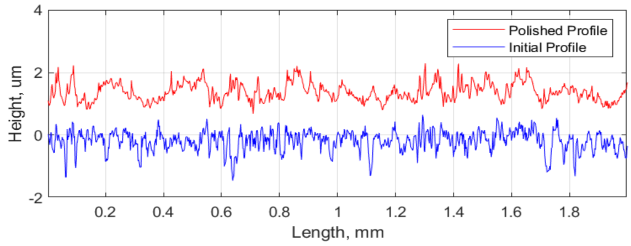

Fig. 4. Center longitudinal profiles of initial (blue) and LRM (red) topographies under stable LRM process.

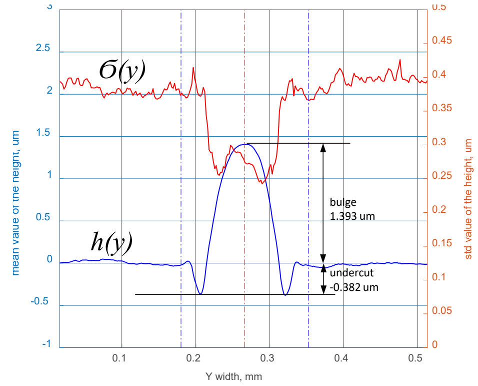

Fig. 5. Transversal profiles of laser track (blue) and standard deviation (red).

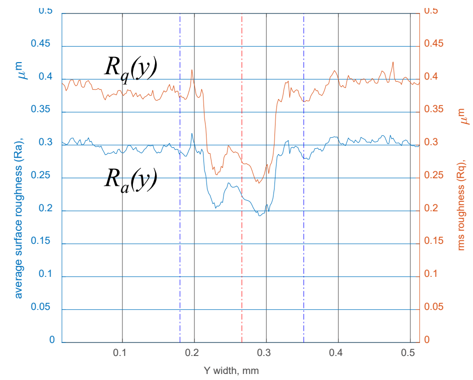

Fig. 6. Transversal profiles of $R_a(y)$ (blue) and $R_q(y)$ (red).

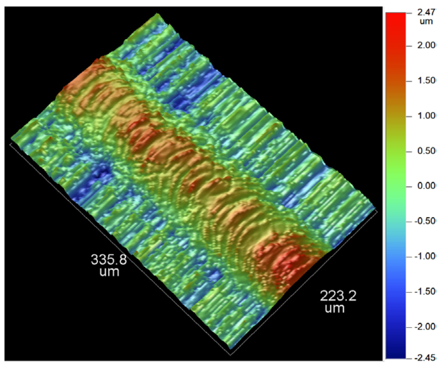

Fig. 7. Detailed view of the ripples formed during a stable LRM process.

This is a resupply of March 2023 as the template used in the publication of the original article contained errors. The content of the article has remained unaffected.

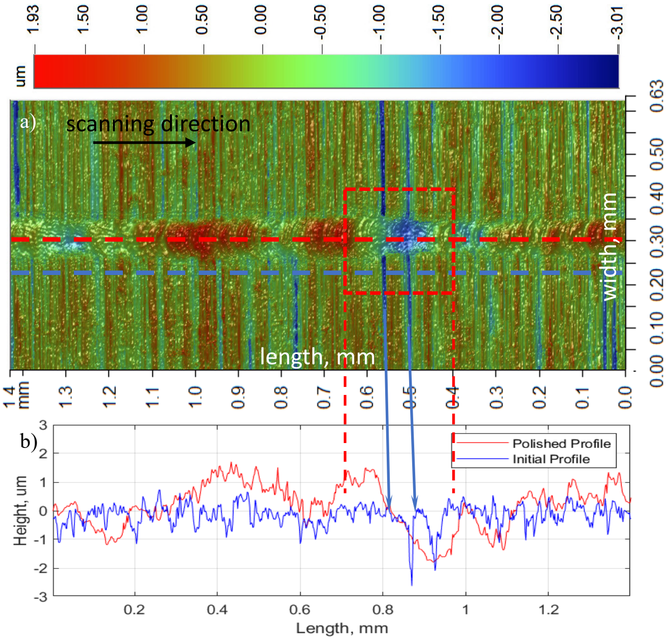

Fig. 8. Effect of initial surface features on topography formation: a) original 3D topography and b) longitudinal profiles (red: remelted, blue: initial).

This is evident from the analysis of the surface topography of line 3 in Tab. 1 (39 to 41 mm) that is presented in Fig. 8. Visual inspection of the topography reveals that the initial surface topography has two deep trenches/troughs of ~7 µm wide and ~2 µm deep that were introduced by the grinding process. While laser passes over these trenches, a noticeable deep cavity/recess (~2 µm) and wide (~80 µm) was formed. It is believed that this a typical example of the effect of the initial surface features on remelted topography formation during the shallow remelting regime. In this example, a bulge with a height of ~1.2 µm rapidly changes into a 2 µm deep cavity because of the presence of two deep trances. After another approximately 100 µm of travel, the bulge was restored to its normal dimensions.

This type of significant variations of the initial topography affect the shape of laser track and surface quality. The bulge height has standard deviation of 0.788 µm, R_a = 0.624 µm, and R_q = 0.787 µm (Fig. 9), all values that are significantly larger than the initial surface topography. The potential effects of process created surface features on the melt pool dynamics during polished line overlap or corrective passes are outside the scope of this study and will be analyzed in the future.

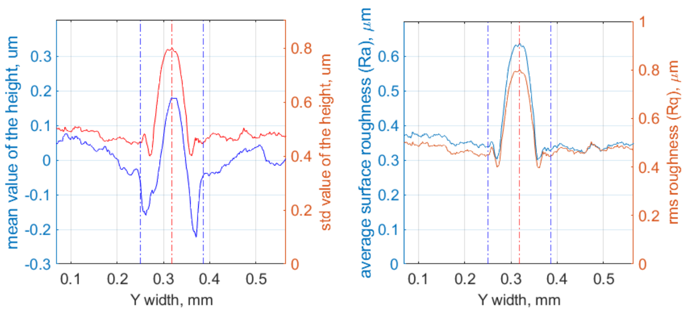

Fig. 9. Surface quality metrics associated with the form of the laser track.

3.3. Effect of thermodynamic instability of the LRM process

A typical example of the effect of thermodynamic instability on the LRM process is shown Fig. 10. This example was taken from line 7 in Tab. 1 (25 to 27 mm). This LRM trial is characterized by an 100% increase in the applied laser power with respect to the uniform formation of the line remelted (40 W vs 20 W power for the stable line). This combination of over-melt process parameters has a much higher energy deposition rate on the material and this leads to formation of more extreme irregularities.

More specifically, at the beginning of the experiment (< 0.7 mm length), LRM process is stable and showcases a typical laser track with a bulge of ~2.5 µm and ripple structures. However, immediately after the 0.7 mm mark, LRM process becomes thermodynamically unstable and appears to lose the previous rapid melting-solidification equilibrium. As a result, the stable regime is lost between 0.7 and 1.1 mm and a cavity with a depth of approximately 11 µm is formed. LRM process consistency is reestablished after the 1.1 mm mark and it leads to the formation of a bulge with a height of about 2.5 µm. This type of significant (~13.5 µm) height variation of the nonuniform surface feature is likely caused by the instant and temporary disappearance of stable melt pool flow characteristics. It is known that stable flows push the molten material backwards thus causing it to pile up in the zone behind the pool [14]. Nonetheless, when the melt pool fluctuates and disperses (0.9 mm location) it will become incapable to push the molten material backwards. By contrast, when melt pool becomes again stable at the 1.1 mm location, it again pushes the material backwards. This succession of events results in a spatially separated cavity followed by a bulge.

Fig. 10 also suggests that once the melt pool loses its stability, the remelted line width becomes unstable as well. This aspect, combined with the high variance of surface height are good indicators of process instability. The STD for this area increased from 0.38 µm to 1.1 µm, thus confirming the strong correlation between process instability and quality loss.

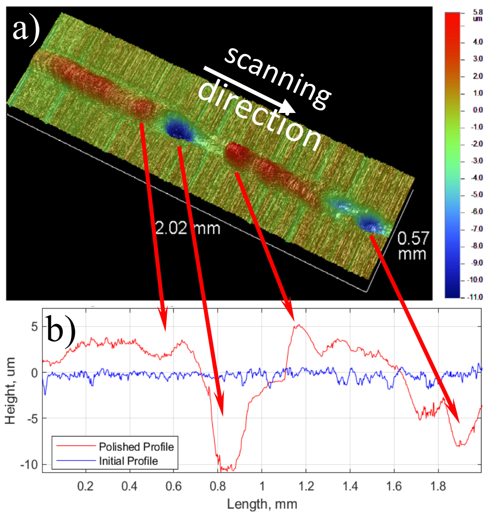

Fig. 10. Effect of thermodynamic instability of the LRM process: a) 3D topography and b) longitudinal profiles.

2. Summary and conclusions

This research work was focused on the preliminary analysis and classification of process-induced surface topography nonuniformities during laser remelting. Throughout this study, several laser remelted tracks were produced with under-melt, stable-melt, and over-melt process conditions. Their surface topographies were analyzed to identify typical topographical nonuniformities and possible sources causing their formation. For this purpose, qualitative and quantitative comparisons were performed between their surface form and quality metrics. Based on this analysis, the following conclusions can be made:

- Laser tracks formed under stable-melt conditions (20 W, 50 mm/s) demonstrated the presence of a typical ripple-structured topography with a bulge height of 1.393 µm and an undercut depth of -0.382 µm. In this case, surface quality improved from $R_{a,ini}$ = 0.31 µm to $R_{a,LMR}$ = 0.22 µm (29.0% improvement) and from $R_{q,ini}$ = 0.40 µm to $R_{q,LMR}$ = 0.27 µm (32.5% improvement). These stable-melt laser tracks and their form and topography parameters were used as a baseline for the subsequent conditions.
- Two main types of topographic nonuniformities formed during LRM were found through visual and statistical identification. While the first category was determined by the initial surface topography during under-melting conditions, the second was caused by unstable thermodynamic laser-material interactions during over-melting.
- The effect of initial surface on remelted topography formation was shown during under-melt conditions (+0.2 mm defocus from the stable-melt). In this case, the presence of two deep surface trenches that were introduced by the prior grinding operation caused the formation of a noticeably deep (~2 µm) and wide (~80 µm) cavity. The bulge height had a high standard deviation of 0.788 µm. Its R_a = 0.624 µm and R_q = 0.787 µm roughness characteristics were significantly larger than those associated with the initial surface topography. This observation can be exploited during future predictive remelting process control/ optimization loops when laser power and/or speed can be adjusted in advance according to known/predetermined locations of significant irregularities on the initial/ground surface.
- The effect of thermodynamic instability of the LRM process was analyzed in conjunction with the over-melt condition (double laser power over the stable-melt). In this case, the LRM process becomes thermodynamically unstable and loses the consistency of rapid melting-solidification equilibrium. The thermal conduction-convection imbalance forms when excessive energy is delivered into the laser-material interaction zone such that the rapid melting process became dominant over the rather slow solidification phenomenon. This effect causes the melt pool to fluctuate its dimensions, to distribute the molten material erratically and to chaotically change its flow characteristics. In case of the example presented in this work, this translated into a cavity with a depth of around 11 µm. The potential occurrence of this effect should be taken into consideration by avoiding the over-melt conditions.

The results obtained open new research avenues toward the in-process prediction of surface topography formation and evolution via online monitoring and predictive control/optimization of the LRM process stability.

Acknowledgements

The work presented in this study is the result of the collaboration between National Research Council of Canada and Western University (Canada) under Canada-Germany 3+2 International Consortium project. Partial financial support was also provided by the Natural Sciences and Engineering Research Council (NSERC) of Canada.

References

[1] Willenborg E. Polishing with laser radiation. In: Poprawe R, editor, Tailored Light 2: Laser Application Technology. Springer; 2011. Chap. 11.3.
[2] Temmler A, Willenborg E, Wissenbach K., Design surfaces by laser remelting. Physics Procedia 2011; 12:419-30.
[3] Bordatchev EV, Hafiz AMK, Tutunea-Fatan OR. Performance of laser polishing in finishing of metallic surfaces. International Journal of Advanced Manufacturing Technologies 2014; 73:35-52.
[4] Nüsser C, Kumstel J, Kiedrowski T, Diatlov A, Willenborg E. Process- and material-induced surface structures during laser polishing, Advanced Engineering Materials 2015; 17(3):268-77.
[5] Bordatchev EV, Cvijanovic SJ, Tutunea-Fatan OR. Preliminary experimental analysis of the surface topography formation during laser polishing H13 tooling steel using statistical characteristics of the surface amplitude distribution. Procedia Manufacturing 2020; 48:159-64.
[6] Miller JD, Tutunea-Fatan OR, Bordatchev EV. Experimental analysis of laser and scanner control parameters during laser polishing of H13 steel. Procedia Manufacturing 2017; 10:720-9.
[7] Bordatchev EV, Cvijanovic SJ, Tutunea-Fatan OR. Effect of initial surface topography during laser polishing process: Statistical analysis. Procedia Manufacturing 2019; 34:269-74.
[8] Nüsser C, Kumstel J, Kiedrowski T, Diatlov A, Willenborg E. Process- and material-induced surface structures during laser polishing. Advanced Engineering Materials 2015; 17(3):268-77.
[9] Anthony TR, Cline HE. Surface rippling induced by surface-tension gradients during laser surface melting and alloying. J. Applied Physics 1977; 48:3888-94.
[10] Avanesov VS, Zuev MA. Investigation of surface topology after melting by laser beam. Proceedings of the SPIE 1996; 2713:340-3.
[11] Ramos-Grez JA, Bourell DL. Reducing surface roughness of metallic freeform-fabricated parts using non-tactile finishing methods. Int. J. Materials and Product Technology 2004; 21(4):297-316.
[12] Xu J, Zou P, Kang D, Wang W. Theoretical and Experimental Study of bulge formation in laser polishing of 304 stainless steel. Journal of Manufacturing Processes 2021; 66:39–52.
[13] Temmler A, Liu D, Preußner J, Oeser S, Luo J, Poprawe R, Schleifenbaum JH. Influence of laser polishing on surface roughness and microstructural properties of the remelted surface boundary layer of tool steel H11. Materials & Design 2020; 192: paper 108689, 25 p.
[14] Guo Q, Qu M, Escano LI, Hojjatzadeh SM, Young Z, Fezzaa K, Chen L. Revealing melt flow instabilities in laser powder bed fusion additive manufacturing of aluminum alloy via in-situ high-speed X-ray imaging. Int J of Machine Tools and Manufacture 2022; 175: paper 103861, 10 p.

This is a resupply of March 2023 as the template used in the publication of the original article contained errors. The content of the article has remained unaffected.